Determination of the packing fraction of silica nanoparticles from the rheological and viscoelastic measurements of nanofluids

Rosa Mondragon[1], J. Enrique Julia[2], Antonio Barba[1], Juan Carlos Jarque[1,*]

[1] Instituto de Tecnología Cerámica. Universitat Jaume I.
Campus de Riu Sec. 12071-Castellón de la Plana. Spain

[2] Departamento de Ingeniería Mecánica y Construcción. Universitat Jaume I
Campus de Riu Sec. 12071-Castellón de la Plana. Spain

* Corresponding author. E-mail: juancarlos.jarque@itc.uji.es. Tel: +34 964 342424

Abstract

Nanofluids have become of great interest due to the excellent properties and reduced size of nanoparticles making them useful for different applications. The agglomeration of nanoparticles depends on the interparticle interactions. To determine the degree of agglomeration of particles in silica nanofluids the rheological and viscoelastic behavior was used. Nanofluids at different volume fractions (φ = 0.002-0.132) and *pH* values (2, 7 and 10) were prepared. Final packing of particles at each *pH* condition was obtained from the modeling of viscosity data to the Quemada equation using effective volume fractions for the first time. Similar equations were proposed by the authors to model the elastic and viscous moduli and the same packing fractions were obtained. The densest packing is achieved at the isoelectric point where particles are uncharged (φ_m = 0.33). Higher surface charges generate looser packing. Packings are always lower than for hard spheres due to the cohesive forces.

Key words: nanofluids, rheology, viscoelasticity, particle packing, nanostructure

1 Introduction

Nanoparticles are considered as important raw materials for future nanotechnology applications due to their excellent electrical, optical and mechanical properties and their unique characteristics because of their reduced dimension. Nanofluids (fluids with suspended nanoparticles (Choi, 1995)) have become of great importance in many applications because of their high stability (Bergna and Roberts, 2006; Iler, 1979). The fact of remaining for very prolonged periods of time without significant settling or loss of stability has made nanofluids suitable for paints, dyes, ceramics, coatings, etc.

In the range size of the nanofluids, the ratio particle surface to particle volume is so high that all the interactions are controlled by short-range forces: Van der Waals attraction, electrostatic repulsion, esteric repulsion and solvation forces. The stability and agglomeration of particles depend on the total interparticle interactions which can be changed by modifying the ionic strength and the *pH* of the suspension (Bergna and Roberts, 2006; Iler, 1979; Quemada and Berli, 2002; Shaw, 1991).

The rheological and viscoelastic behavior of nanofluids is affected by the colloidal forces present between particles (Amiri et al., 2009; Quemada and Berli, 2002). When solid content is increased there are more particles per unit volume and the colloidal interactions increase due to the proximity of neighbour particles. Hence, the key parameter characterizing the microstructure is the volume fraction, φ, which represents the volume space occupied by the particles in relation to the total volume.

At low volume fractions the mean distance between particles is large compared to the particle radius. Thus particles are able to move freely driven by the Brownian motion. Under these conditions nanofluids behave Newtonian (the viscosity is independent of the shear rate applied) and 'like liquid' (the viscous modulus, *G''*, is higher than the elastic modulus, *G'*). At high volume fractions the particle movement is constricted by the neighbour ones and the hydrodynamic interactions become important. Under these conditions particles agglomerate and nanofluids behave shear thinning (Quemada and Berli, 2002; Chen et al., 2005, 2007). This shear dependent behavior is due to the clusters, agglomerates, flocs or clusters of flocs that break into primary flocs or individual particles as the shear rate is increased leading to the concept of sheardependent structure (Quemada, 1998). Moreover, these nanofluids present an apparent

yield stress that can be used to analyze the degree of agglomeration. When the presence of these agglomerates is important, nanofluids behave virtually 'like solid' (the elastic modulus, *G'*, is higher than the viscous modulus, *G''*).

At a certain volume fraction a disorder-order transition takes place. This volume fraction at which the transition occurs is known as fluidity limit, φ_m (Russel, 1989; Shapiro and Probstein, 1992). Below this value the nanofluid behaves like a liquid (disordered phase) while above the fluidity limit the nanofluid has the properties of a solid (ordered phase). In colloidal systems exist disorder-order transitions driven by entropic effects in systems dominated by repulsive interparticle potentials and fluidsolid transitions caused by weak attractions.

The graphical representation of viscosity versus the volume fraction allows obtaining the fluidity limit, concentration at which the viscosity takes infinite value. Krieger and Dougherty (Krieger and Dougherty, 1959) proposed an equation to model the viscosity of numerous suspensions with particles different in nature:

$$\eta_r = \frac{\eta}{\eta_F} = \left(1 - \frac{\varphi}{\varphi_m}\right)^{-q} \text{ with } q = [\eta]\cdot\varphi_m \quad (1)$$

where η_r is the relative viscosity, η, is the viscosity of the nanofluid, η_F is the viscosity of the base fluid, $[\eta]$ is the intrinsic viscosity and φ_m is the fluidity limit.

In 1977 Quemada (Quemada, 1977) obtained an expression of the same type but with constant q value, $q = 2$:

$$\eta_r = \left(1 - \frac{\varphi}{\varphi_m}\right)^{-2} \quad (2)$$

This equation was obtained from a minimum principle applied to the energy dissipated by viscous effects.

These equations were developed for hard spheres systems and have been used successfully to model experimental data of micrometrical particles (Hurisz and Cochran 2003; Loebbecke et al., 2009; Nagel et al., 2002). Some authors (Chen et al., 2005, 2007; Chen et al., 2010; Solomon and Boger, 1998; Tseng and Wu, 2002) have applied equations directly to model experimental data obtained for different nanoparticles systems: silica, silver, hematite. However, in the case of nanosize range, the packing fractions obtained are very low because these equations have to be modified to apply

them for nanoparticles systems. In this case the volume fraction has to be substituted by an effective volume fraction that takes into account the effective radius of the nanoparticles (Amoros et al., 2010; Ponton et al., 1996; Quemada, 1998):

$$\eta_r = \left(1 - \frac{\varphi_{eff}}{\varphi_m}\right)^{-q} \quad (3)$$

The effective radius results from the electrical double layer formed around particles when stabilized electrostatically and is expressed as follows:

$$r_{eff} = r_p + \kappa^{-1} \quad (4)$$

where r_p is the particle radius and κ^{-1} is the thickness of the electrical double layer. From these values the effective volume fraction for spherical particles is the following:

$$\varphi_{eff} = \varphi \left(\frac{r_{eff}}{r_p}\right)^3 \quad (5)$$

The intrinsic viscosity, [η], depends on the morphology of the particles or agglomerates if they are the flow units (Rubio-Hernandez et al., 2006). For spherical particles its value is established at 2.5 while for non-spherical particles or clusters can achieve values up to 14.

The fluidity limit, φ_m, corresponds to the maximum packing fraction implying that the suspension cannot be packed in a denser fashion. When the liquid contained in a suspension is removed progressively the solid content of the suspension is increased an the particles rearrange up to the instant in which the fluidity limit is achieved and the jamming of the particles takes place. The resultant structure is indeed of random structure and corresponds to the final arrangement that particles will present.

In particulate systems two packing states can be found, related to the critical structural changes, when dry particles are packed under gravity: the random close packing (RCP) represents the densest packing state that uniform spheres can achieve when randomly packed, while the random loose packing (RLP) is referred as the least dense packing that can resist an external load (Dong et al., 2006, 2009; German, 1989). For hard, monodispersed, spherical particles with micrometrical size the final volume fractions achieved at each packing state are established at φ_{RCP}= 0.64 and φ_{RLP}= 0.56. However, these values depend on the particle size and the interparticle forces present in the system.

Although there no exists a rigorous correspondence between the fluidity limit, φ_m, and the critical packing fraction for dry particles, φ_{RCP}, some author establish that for spherical, rigid, monodisperse and without surface forces particles, the fluidity limit is close to the RCP (Brady, 1993; Quemada, 1998). However, polydispersity in size, shape or surface charge, strongly affects the distribution of particles and hence the order disorder transitions (Quemada and Berli, 2002). In these cases in which there are more factors influencing the packing of particles, the final packing state achieved for suspensions can differ from that obtained for dry paricles.

For particles in the nanometrical size range, the Van der Waals cohesive forces become dominant. This force restricts the relative movement of the particles resulting in the formation of agglomerates that affects the packing particles. Hence, the volume fraction for random close packing depends on the Hamaker constant and the particle size (Dong et al., 2006; Forsyth et al., 2001; Yu et al., 2003). This influence of the interparticle forces obtained in packing experiments under gravity, can be applied to the packing of particles inside a suspension. In this way, the fluidity limit depends on the surface forces which include not only the Van der Waals attractive forces due to the small particle size, but also the electrostatic repulsive forces generate to change the stability of the nanofluids.

When nanofluids are electrostatically stabilized the presence of repulsive forces and the electrical double layer also affects the packing state due to the electroviscous effects that make the viscosity to increase as a consequence of the electrical double layer. The effect influencing the fluidity limit is the secondary electroviscous effect. It produces an increase of the viscosity due to the overlap of electrical double layers, modifyin the final packing fraction of the particles at the jamming point (Anoop et al., 2009; Hunter, 1988). In this way high repulsions generate loose structures with low packing. The phase transition takes place at volume fractions even lower than in the presence of cohesive forces. Therefore, the variables that modify the total interactions, like *pH*, also modify the final packing fraction.

Another factor influencing the final packing state is the capillary force acting on particles when limited water content is present. This cohesive force difficult the particles rearrangement and lead to lower packing fractions. In this case, the disorderorder transition takes place earlier at lower volume fractions (Yu et al., 1997; Feng and Yu, 2000; Xu et al., 2004). In nanofluids, if it is considered a process in which the solid

content is increases through the continuous removal of water, capillary forces will be present at the last stage of the packing process and the final arrangement of the particles will be influenced by this force.

The fluidity limit obtained from the viscosity-effective volume fraction curve, can be also obtained from the graphical representation of the elastic modulus, *G'*, the viscous modulus, *G''*, or the complex viscosity, η^*, versus the effective volume fraction. The experimental data can be modeled following an equation similar to the Krieger-Dougherty one.

In this work the rheological and viscoelastic behavior were studied for different solid contents and *pH* values. Quemada equation was used to model experimental data of viscosity and new equations were proposed to model elastic and viscous moduli using effective volume fractions. The maximum packing fractions (φ_m) and the intrinsic viscosity for each *pH* value were obtained from the model.

The information obtained in this study has been used in a later work to determine the packing fraction and the related properties (porosity, microstructure and mechanical properties) of nanostructurated grains obtained by drying single droplets of nanofluids. The importance of the spray drying in different applications makes the characterization of the powder properties very useful.

2 Experimental techniques

The following sections offer a description of the experimental techniques used to measure all the properties of the nanofluids.

Zeta potential, ψ

The zeta potential was measured using a Zetasizer Nano ZS (Malvern Instruments) from the electrophoretic mobility of particles when an electric field is applied. This velocity is measured using Laser Doppler Velocimetry (LDV) and the zeta potential is obtained through the Henry equation (Chen et al., 2005).

Debye length, κ^{-1}

The following equation can be used to link the thickness of the electrical double layer and the ionic strength for a symmetrical electrolyte in aqueous solution:

$$\kappa = 0.215 \cdot 10^{-9} \cdot \sqrt{I}\, I \quad (6)$$

where I is the ionic strength of the medium, which is calculated from the electrical conductivity. Griffin and Jurinak (1973) obtained the following empirical equation to calculate the ionic strength in suspensions in which sodium and chloride ions are present:

$$I = 0.013 \cdot EC \quad (7)$$

where EC is the electrical conductivity of the suspension, which was measured directly using an EC-Meter Basic 30+ conductimeter (Crison).

Viscosity, η

The viscosity and rheological behavior of nanofluids were obtained by conducting tests under steady state conditions using a Bohlin CVO-120 rheometer. A double gap (DG 40/50) device composed of two concentric cylinders suitable for low viscosity suspensions was used. Before each test, a pre-treatment was applied to the nanofluids for 30 seconds to ensure similar starting conditions for all the samples.

Elastic modulus and viscous modulus, G', G''

The elastic modulus and viscous modulus (also known as storage and loss moduli, respectively) were obtained by conducting tests under dynamic oscillatory conditions using a Bohlin CVO-120 rheometer. A cone/plate (CP4º/40) device composed of a flat plate and a cone was used. First, strain sweep tests were carried out at a constant frequency in order to establish the linear viscoelastic region in which the strain does not influence the value of the modules. Finally, frequency sweep tests at a constant strain were performed.

3 Materials

All the experiments were carried out with silica nanofluids. In this work, commercial fumed silica provided by Degussa was used. Fumed silica produced by flame hydrolysis of chlorosilane ($SiCl_4$) is the most hydrophilic silica and an extremely versatile material which also has unique properties. The silica chosen was an Aerosil 200 consisting in amorphous hydrophilic silica nanoparticles with primary units of 12 nm and a density of 2200 kg/m^3 according to the manufacturer.

The nanoparticles were acquired in dry powder form and they were observed by means of scattering electron microscopy (SEM). It can be seen in Figure 1 a) that the

nanoparticles form agglomerate of micrometrical size, larger than the primary particles. Therefore, when dispersing them with water, it is very important to break the agglomerates down into the primary nanoparticles (observed in Figure 1 b)), or the smallest agglomerate size if well dispersed suspensions are require. Figure 1 c) shows the final agglomerates obtained in a well dispersed nanofluid, observed by transmision electron microscopy (TEM).

3.1 Characterization of nanoparticles

Initially, the nanoparticles were characterized in terms of their specific surface and isoelectric point.

First, the specific surface was measured using a TriStar 3000 instrument (Micrometrics). This equipment determines the specific surface of powder samples by adsorption of nitrogen gas using the BET method. It was obtained experimentally a value for the specific surface of 211±7 m^2/g. This value is in good agreement with the specific surface provided by the manufacturer, which has a value of 200 ± 25 m^2/g.

On the other hand, the isoelectric point was obtained from the zeta potential curves. The zeta potential represents the electrostatic potential of the particles and it is proportional to their surface charge. The isoelectric point is the *pH* value at which the surface charge and the zeta potential take a value of zero. To determine the isoelectric point of the silica nanofluids the zeta potential of suspensions prepared under different *pH* conditions was measured. All the measurements were carried out in dilute suspension.

Figure 2 shows the variation of zeta potential with *pH.* It can be seen that the isoelectric point corresponds approximately to *pH* = 2. When the *pH* is increased above this value, particles become negatively charged while at *pH* values lower than the isoelectric point, the free protonated water forms positive groups.

3.2 Preparation of nanofluids

Nanofluids with different particle concentrations were prepared by adding distilled water to the defined amounts of nanoparticles. In this method, known as the two-step method, the nanoparticles are purchased as dry powder and then dispersed in the liquid medium. The solid content is expressed in terms of mass fraction (w/w) which represents the weight of solid respect to the weight of the suspension.

The dispersion was performed using an ultrasonic probe (UP400s from Hielscher Company) that has been checked to be the most effective dispersion system (Pastoriza-Gallego et al., 2009; Petzold et al., 2009). Initially, the mixture of nanoparticles with the water was submitted to a sonication treatment for a period of time. After that, the *pH* of the nanofluid was modified by adding HCl or NaOH solutions (0.01 w/w). Finally, to ensure correct dispersion of all the components, the nanofluids are submitted to a second sonication treatment for 2 minutes.

To determine the period of time necessary to disperse the nanoparticles, the influence of the first sonication time on the viscosity was obtained for suspensions at Ys = 0.20 w/w and *pH* = 10. Figure 3 shows the evolution of the viscosity at different shear rates with the total sonication time, taking into account both the first sonication time and the 2-minute treatment performed after *pH* adjustment. It can be seen that even for the worst condition at high solid content, after 5 minutes (3 + 2 minutes) the viscosity does not change significantly. Moreover, the differences in viscosity depending on the shear rate for a constant time are negligible after 5 minutes. Therefore, this was the time chosen to carry out all the tests.

4 Results and discussion

Suspensions at different solid contents (volume fractions from 0.002 to 0.132) were prepared for three *pH* values (2, 7 and 10). The value of *pH*=2 corresponds to the isoelectric point as mentioned above and the Van der Waals forces are predominant. At *pH*=7 and *pH*=10 nanofluids are electrostatically stabilized and particles present negative surface charge.

Rheological and viscoelastic behavior were determined at 25 ºC under these conditions. From the viscosity and the elastic and viscous moduli results the fluidity limits and, hence, the maximum packing fractions were obtained.

4.1 Rheological behavior

For each nanofluid prepared the rheogram was obtained as shown in Figure 4. Two of the parameters most widely used to analyze the degree of agglomeration are the extrapolated yield stress, σ_Y, and the plastic viscosity, η_P, (Amoros et al., 2010). These parameters can be obtained adjusting the shear stress/share rate curve obtained during the viscosity test to the Bingham model:

$\sigma = \sigma_Y + \eta_P \cdot \gamma$ (8) where σ is the shear stress applied and γ is the shear rate generated. In Table 1 it can be seen that for low solid contents nanofluids present Newtonian behavior without yield stress. That means that nanoparticles forms stable agglomerates which are independent of the shear rate applied. For solid contents higher than 0.069 v/v nanofluids present yield stress and behave shear-tinning (shear dependent structure). When the solid content is increased, the hydrodynamic interactions as well as the probably of collision become important, enhancing the aggregation processes. Hence, the increase in solid content leads to an increase in the degree of agglomeration of the particles and as a consequence the stress required for the suspensions to flow is also increased. To model the viscosity results with the solid content, effective volume fractions are needed. When nanoparticles are electrostatically stabilized surface charges appear forming an external double layer around the particles. The thickness of this layer depends on the presence of electrolytes and ions introduced in the nanofluids when adjusting the *pH* value (introduction of chloride and sodium ions with HCl and NaOH respectively). The use of effective volume fractions allows screening the effect of the electrolyte concentration on the viscosity to model the experimental data. The thickness of the electrical double layer o Debye length was calculated from the electrical conductivity measurements of each nanofluid by means of equations 6 and 7. Table 2 shows the values obtained for the electrical double layer. With these values and equations 4 and 5 the effective volume fractions were calculated taking for the particle radius a value of 6 nm. Final values are also shown in Table 2. As can be seen the effective volume fraction is always higher than the theoretical one due to the higher effective particle radius. Finally the relative viscosity was obtained. For Newtonian nanofluids the viscosity is constant while for shear thinning nanofluids the viscosity at low shear rate ($\gamma = 1\ s^{-1}$) was chosen. It is at low shear rates where nanoparticles are agglomerate and the information about the packing particle is given. For the base fluid (distilled water) the theoretical value of 0.001 Pa·s was taken. Experimental data were modeled according to the modified Quemada equation (Equation 3 with q=2). Table 3 shows the fluidity limits and the intrinsic viscosity obtained from the model for each *pH* condition. In Figure 5 experimental data are

represented together with the theoretical curves corresponding to the Quemada equation. It can be seen that the viscosity results are in good agreement with the model. Moreover, for high volume fraction errors bars are also represented. These errors were obtained from the standard deviation of four different measurements for each experimental condition.

As can be seen the fluidity limit, φ_m, increases as the *pH* value decreases. The packing fraction is a parameter that depends on the nanofluid conditions and the interparticles forces presents in it. The *pH* value is one of the parameters most commonly used to stabilize a nanofluid by modifying the surface forces acting on the particles. When the *pH* value is increased, particles get negative charge and an electrical layer is formed around them. The repulsion generated due to the overlap of the electrical layers of particles approaching each other leads them to remain apart (Hunter, 1988). This effect, known as secondary electroviscous effect, modifies the volume fraction at which the disorder-order transition (liquid-solid phase change) takes place (Russel et al, 1989). The increase in the *pH* value results in higher viscosities and loose packings as a consequence of the repulsion between particles.

For *pH*=2 (corresponding to the isoelectric point), only Van der Waals attractive forces are present and the maximum fluidity limit is achieved (φ_m = 0.33). In this case, when particles approach each other they trend to form agglomerates more compact because there is no repulsion between them. Therefore, the fluidity limit at the isoelectric point represents the maximum packing fraction for this particulate system. This value is lower than the 0.64 predicted for the RCP of hard, monodispersed spheres packed under gravity. In this case, particles are in suspension and Van der Waals cohesive forces are predominant due to the particle size. These forces restrict the relative movement of particles resulting in agglomerates with presence of large pores and worst packings than in the case of hard spheres.

For the intrinsic viscosity, $[\eta]$, its value increases with the *pH* of nanofluids. This parameter depends on the morphology of particles or agglomerates. For hard, spherical particles takes a value of 2.5 which increases as the morphology is modified. In this system, at *pH* = 2, where attractive forces are predominant, particles agglomerate resulting in more compact clusters. This condition present the lower intrinsic viscosity ($[\eta]$ = 6.15). As the *pH* value is increased, repulsion between particles leads them to

form chain like structures less spherical, increasing the intrinsic viscosity of the system (Rubio-Hernandez et al., 2006).

4.2 Viscoelastic behavior

From the measurements of viscoelastic behavior, the evolution of each modulus with the oscillation frequency was obtained as can be seen en Figure 6. This behavior is also used to determine if the nanofluids behave like a liquid with well dispersed particles or behave like a solid with agglomerates that leads to gel formation. It can be observed that for all the nanofluids prepared the viscous modulus is higher than the elastic one. That means that the viscous part is predominant and all the suspensions behaves like a liquid. These suspensions follow the viscoelastic liquid model proposed by Maxwell (Barnes et al., 1989). In this model the elastic modulus is proportional to the squared frequency while the viscous modulus is proportional to the frequency. This potential law is followed by all nanofluids. Only under the highest solid content conditions for each *pH* series, nanofluids slightly differ from the like liquid behavior although they do not behave like solid.

It can also be seen in Figure 6 that both moduli increase with solid content. Evolution of individual values of elastic modulus and viscous modulus with the effective volume fraction can be also used to determine the maximum packing fractions at each condition. Experimental data can be modeled according to a theoretical equation similar to the Krieger Dougherty one, using relative values of the moduli. Following equations have been proposed by the authors to model the experimental results and to obtain the maximum packing fraction of the particles:

$$G'_r = \frac{G'}{G'_F} = \left(1 - \frac{\varphi_{eff}}{\varphi_m}\right)^{-b'} \quad (9)$$

$$G''_r = \frac{G''}{G''_F} = \left(1 - \frac{\varphi_{eff}}{\varphi_m}\right)^{-b''} \quad (10)$$

where G'_F and G''_F are the elastic and viscous moduli of the base fluid respectively.

To model the results, individual values are needed. In this work the values were taken at a constant frequency of 0.0044 Hz where there is less variability in the measurements. The values for the base fluid (distilled water) have also measured experimentally: $G'_F = 1.57 \cdot 10^{-6}$ Pa, $G''_F = 1.18 \cdot 10^{-4}$ Pa.

Tables 4 and 5 show the values obtained for the maximum packing fraction and the parameters *b'* and *b''* resulting from the model of the elastic modulus and the viscous modulus respectively. It can be seen that these values are the same obtained from the fitting of the viscosity data to the Quemada equation. The best packing (RCP) is produced at *pH* = 2 (φ_m = 0.32 and φ_m = 0.31 from elastic and viscous moduli respectively) while an increasing in the *pH* value and the repulsive forces present leads to worse packings with looser structures.

For a fixed solid content, and the packing fraction corresponding to each *pH* value, the higher the parameter (*b', b''*), the higher the modulus (*G', G''*). As a results, the relationship between the parameters *b'* and *b''* is related to the relationship between the moduli *G'* and *G''*. Therefore, the fact that *b''* is higher than *b'* means that the viscous modulus, *G''*, is higher than the elastic modulus, *G'*, and all the suspensions behave like a liquid. In this work, it can be observed from the results that the parameter *b'* corresponding to the elastic modulus model, takes a value around 0.85 for the three systems studied. In the case of viscous modulus, the parameter *b''* takes a value around

1.00. That means that for all the suspensions analyzed the viscous character is predominant and all of them behave like a liquid.

In Figure 7 a) and b) experimental data are represented together with the theoretical curves corresponding to the model for the elastic modulus and the viscous modulus respectively. It can be seen that the results are in good agreement with the model.

4.3 Complex viscosity

Elastic and viscous moduli define a complex function known as shear complex modulus, G^*, which can be expressed as follows: $G^*(i\omega) = G'(\omega) + G''(\omega) \cdot i$ (11)

where ω is the oscillation frequency. From this complex modulus, a complex viscosity, η^*, that relates the elastic and viscous parts of nanofluid with the oscillation frequency is obtained: *G*

$$\eta^* = \eta' - \eta'' \cdot i = \frac{G''}{\omega} - \frac{G'}{\omega} \cdot i \quad (12)$$

The evolution of the complex viscosity of all nanofluids with the oscillation frequency was measured as shown in Figure 8. It can be observed that complex viscosity changes with solid content and *pH* value in the same way that the nanofluid

viscosity. Hence, relative values of complex viscosity (related to water: η^* = 0.001 Pa·s) can be modeled according to Quemada equation like the viscosity. To obtain the maximum packing fractions and intrinsic viscosities for each system individual values of complex viscosity at a frequency of 0.0044 Hz were taken.

Table 6 shows the values obtained for the maximum packing fraction and the intrinsic viscosity resulting from Quemada equation. It can be seen that these values are the same obtained from the fitting of the viscosity and the elastic and viscous moduli to the models proposed. The best packing is produced at *pH* = 2 (φ_m = 0.33) while an increasing in the *pH* value and the repulsive forces present leads to worse packings with looser structures. The intrinsic viscosity increases with the *pH* value. At *pH* = 2 ($[\eta]$ = 6.07) attractive forces are predominant and more spherical agglomerates are formed, while an increase in the electrostatic charge produces electroviscous effects that generate chain like structures with higher intrinsic viscosities.

Figure 9 shows the good agreement between the experimental data and the theoretical curves corresponding to the modeling of the complex viscosity.

5 Conclusions

Silica nanofluids at different solid contents and *pH* values were prepared and studied. Rheological and viscoelastic behavior were analyzed from the measurement of the viscosity, and the elastic and viscous modulus.

For low solid contents up to 0.069 v/v nanofluids are well dispersed and behave Newtonian without apparent yield stress. Higher solid contents leads to an increase in the particle interaction and agglomerates are formed. As a result nanofluids become shear thinning and an apparent yield stress appears. Moreover, in all cases the elastic modulus is lower than the viscous modulus. This means that the viscous part is predominant and nanofluids behave like a liquid.

Experimental data of low shear rate viscosities were modeled using the Quemada equation. In order to apply this model to nanoparticulate systems, effective volume fraction are needed. The maximum packing fraction for each *pH* value was obtained. The densest packing is achieved at *pH* = 2 when particles are not charged (isoelectric point). The reduced size of nanoparticles generates lower packings than in micrometrical systems due to the Van der Waals forces that predominate. An increase in the *pH* value and the surface charge result in looser packings due to electroviscous effects. In addition, higher surface charges leads to chain like clusters with higher

intrinsic viscosities, while at the isoelectric point agglomerates are more spherical and the intrinsic viscosity in the lowest.

An equation similar to the Krieger-Doughery one was proposed to model the elastic and viscous moduli. Experimental data are in good agreement with the equations proposed. As a result, the same packing fractions were obtained for each *pH* value.

Finally, Quemada equation was used to model the complex viscosity results. Like in the other properties, experimental data can be well described by the theoretical equation and the same packing fractions and intrinsic viscosities were obtained.

As a conclusion, the maximum packing fraction for silica nanoparticles suspended in water is achieved at a volume fraction of 0.33. In later studies of drying of droplets to obtain nanostructurated granules, the authors have checked that this value corresponds to the compacity of the particles inside the crust formed and determines the degree of hollowness of the granules. These results will be published in a future paper.

Acknowledgments

R. Mondragón thanks the Spanish Ministry of Education for a pre-doctoral fellowship (FPU program, Ref. AP2008-01077).

The authors gratefully acknowledge the financial support from the Spanish Ministry of Science and Innovation (projects CTQ2010-21321-C02-01 and CTQ2010-21321-C0202).

References

Amiri, A., Oye, G., Sjöblom, J., 2009. Influence of pH, high salinity and particle concentration on stability and rheological properties of aqueous suspensions of fumed silica. Colloids and surfaces A: Physicochemical Engineering Aspects 349, 43-54.

Amoros, J.L., Berltran, V., Sanz, V., Jarque, J.C., 2010. Electrokinetic and rheological properties of highly concentrated kaolin dispersions: influence of particle volume fraction and dispersant concentration. Applied Clay Science 49, 33-43.

Anoop, K.B., Kabelac, S., Sundararajan, T., Das, S.K., 2009. Rheological and flow characteristics of nanofluids: influence of electroviscous effects and particle agglomeration. Journal of Applied Physics 106, 034909.

Barnes, H.A., Hutton, J.F., Walters, D.K., 1989. An introduction to rheology, Elsevier.

Brady, J.F., 1993. The rheological behavior of concentrated colloidal dispersions. Journal of Chemical Physics 99, 567-581.

Bergna, H.E., Roberts, W.O., 2006. Colloidal silica: Fundamentals and applications, CRC Taylor & Francis.

Chen, S., Oye, G., Sjöblom, J., 2005. Rheological properties of aqueous silica particle suspensions. Journal of Dispersion Science and Technology 26, 495-501.

Chen, S., Oye, G., Sjöblom, J., 2007. Effect of pH and salt on rheological properties of aerosol suspensions. Journal of Dispersion Science and Technology 28, 845-853.

Chen, C.N., Huang, C.T., Tseng, W.J., Wei, M.H., 2010. Dispersion and rheology of surfactant-mediated silver nanoparticles suspensions. Applied Surface Science 257, 650-655.

Choi, U.S., 1995. Enhancing thermal conductivity of fluids with nanoparticles. ASME FED 231, 99-103.

Dong, K.J., Yang, R.Y., Zou, R.P., Yu, A.B., 2006. Role of interparticle forces in the formation of random loose packing. Physical Review Letters 145505.

Dong, K.J., Yang, R.Y., Zou, R.P., An, X.Z., Yu, A.B., 2009. Critical states and phase diagram in the packing of uniform spheres. Europhysics Letters 86, 46003.

Feng, C.L., Yu, A.B., 2000. Quantification of the relationship between porosity and interparticle forces for the packing of wet uniform spheres. Journal of Colloid and Interface Science 231, 136-142.

Forsyth, A.J., Hutton, S.R., Osborne, C.F., Rhodes, M.J., 2001. Effects of interparticle force on the packing of spherical granular material. Physical Review Letters 87, 244301.

German, R.M., 1989. Particle Packing Characteristics. Metal Powder Insdustries Federation, Princeton, New Jersey.

Griffin, G.P., Jurinak, J.J., 1973. Estimation of activity coefficients from the electrical conductivity of natural aquatic systems and soil extracts. Soil Science 116, 26-30.

Hunter, R.J., 1988. Zeta potential in colloid science. Principles and applications, Academic Press Limited.

Hurisz, K.M., Cochran, J.K., 2003. The application of models for high solid content suspensions to pastes. Journal of the European Ceramic Society 23, 2047-2052.

Iler, R.K., 1979. The chemistry of silica: solubility, polymerization, colloid and surface properties, and biochemistry, John Wiley & Sons.

Krieger, I.M., Dougherty, T.J., 1959. A mechanism for non-Newtonian flow in suspensions of rigid spheres. Transaction of the Society of Rheology 3, 137–152.

Loebbecke, B., Knitter, R., Hausselt, J., 2009. Rheological properties of alumina feedstocks for the low-pressure injection moulding process. Journal of the European Ceramic Society 29, 1595-1602. Nagel, A., Petzow, G., Greil, P., 2002. Rheology of aqueous silicon nitride suspensions. Journal of the European Ceramic Society 22, 2805-2812.

Pastoriza-Gallego, M.J., Casanova, C., Paramo, R., Barbes, B., Legido, J.L., Piñeiro, M.M., 2009. A study on stability and thermophysical properties (density and viscosity) of Al_2O_3 in water nanofluid. Journal of Applied Physics 106, 064301.

Petzold, G., Rojas-Reyna, R., Mende, M., Schwarz, S., 2009. Application relevant characterization of aqueous silica nanodispersions. Journal of Dispersion Science and Technology 30, 1216-1222.

Ponton, A., Quemada, D., Lafuma, F., Neel, O., 1996. Studies of rheological behavior of colloidal silica suspensions with interaction potential. Colloids and Surfaces A: Physicochemical and Engineering Aspects 119, 255-259.

Quemada, D., 1977. Rheology of concentrated disperse systems and minimum energy dissipation principle. I. Viscosity-concentration relationship. Rheological Acta 16, 82 94.

Quemada, D., 1998. Rheological modeling of complex fluids. I. The concept of effective volume fraction revised. EPJ Applied Physics 1, 119-127.

Quemada, D., Berli, C., 2002. Energy of interaction in colloids and its implication in rheological modeling. Advances in Colloid and Interface Science 98, 51-85.

Rubio-Hernandez, F.J., Ayucar-Rubio, M.F., Velazquez-Navarro, J.F., Galindo-Rosales, F.J., 2006. Intrinsic viscosity of SiO_2, Al_2O_3 and TiO_2 aqueous suspensions. Journal of Colloid and Interface Science 298, 967-972.

Russel, W.B., Saville, D.A., Schowalter, W.R., 1989. Colloidal dispersions, Cambridge University Press.

Shapiro, A.P., Probstein, R.F., 1992. Random packings of spheres and fluidity limits of monodispere and bidisperse suspensions. Physical Review Letters 68, 1422-1425.

Shaw, D.J., 1991. Introduction to colloid and surface chemistry. Butterworth-Heinemann: Oxford, UK.

Solomon, M.J., Boger, D.V., 1998. The rheology of aqueous dispersions of spindle-type colloidal hematite rods. Journal of Rheology 42, 929-949.

Tseng, W.J., Wu, C.H., 2002. Aggregation, rheology and electrophoretic packing structure of aqueous Al_2O_3 nanoparticle suspensions. Acta Materialia 50, 3757-3766.

Xu, J.Q., Zou, R.P., Yu, A.B., 2004. Packing structure of cohesive spheres. Physical Review E 69, 032301.

Yu, A.B., Bridgwater, J., Burbidge, A., 1997. On the modeling of the packing of fine particles. Powder Technology 92, 185-194.

Yu, A.B., Feng, F.L., Zou, R.P., Yang, R.Y., 2003. On the relationship between porosity and interparticle forces. Powder Technology 130, 70-76.

Figure captions

Figure 1. Nanoparticles of Aerosil 200 observed by SEM and TEM. Figure 2. Evolution of zeta potential with *pH*. Isoelectric point. Figure 3. Evolution of viscosity with sonication time at different shear rates. Figure 4. Rheograms of the nanofluids prepared. (⌘) *pH*=2, (☜) *pH*=7, (⇨) *pH*=10. Figure 5. Evolution of relative viscosity with effective volume fraction and *pH*.
Experimental data and modeled curve.
Figure 6. Evolution of elastic modulus (*G'*: solid symbol) and viscous modulus (*G''*: hollow symbol) with the oscillation frequency. (⌘) *pH*=2, (☜) *pH*=7, (⇨) *pH*=10. Figure 7. Evolution of a) relative elastic modulus and b) relative viscous modulus with
effective volume fraction and *pH*. Experimental data and modeled curve.

Figure 8. Evolution of complex viscosity with the oscillation frequency. (⌘) *pH*=2, (☜) *pH*=7, (⇨) *pH*=10. Figure 9. Evolution of relative complex viscosity with effective volume fraction and
pH. Experimental data and modeled curve.

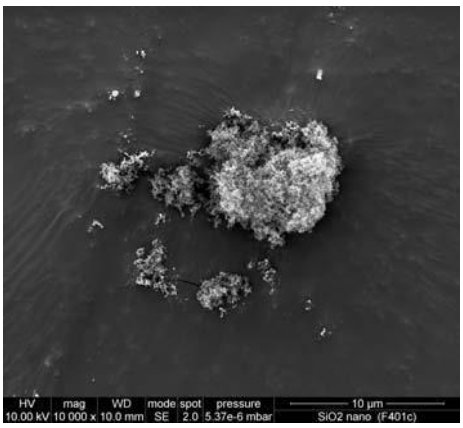

a)

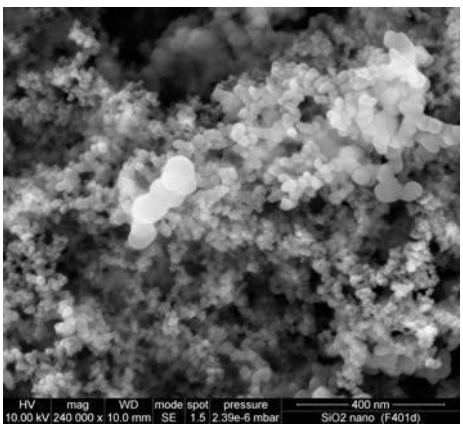

b)

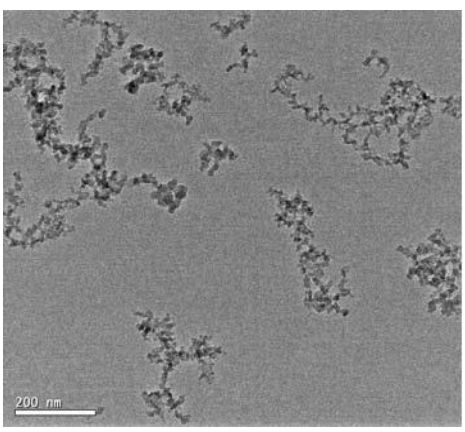

c)

Figure 1. Nanoparticles of Aerosil 200 observed by SEM and TEM.

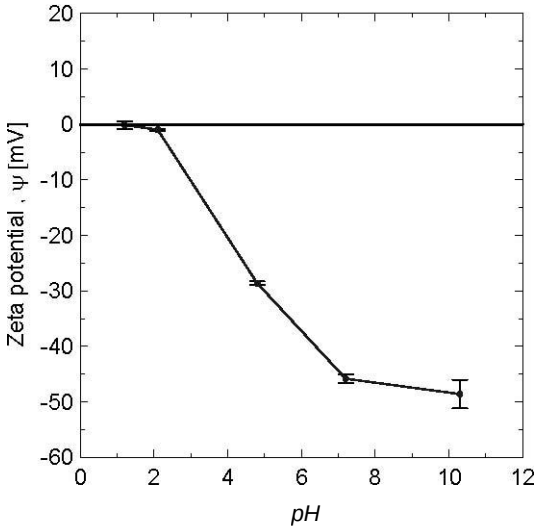

Figure 2. Evolution of zeta potential with *pH*. Isoelectric point.

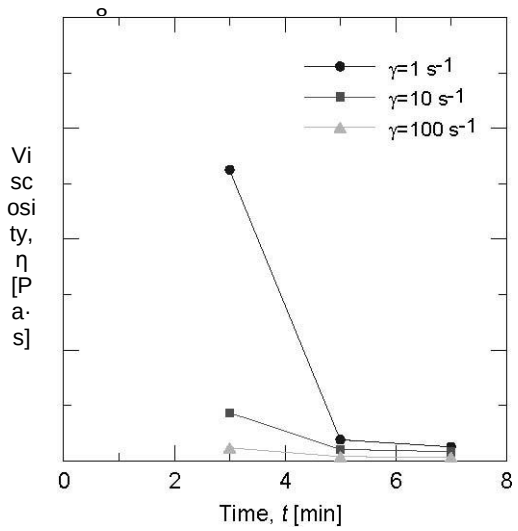

Figure 3. Evolution of viscosity with sonication time at different shear rates.

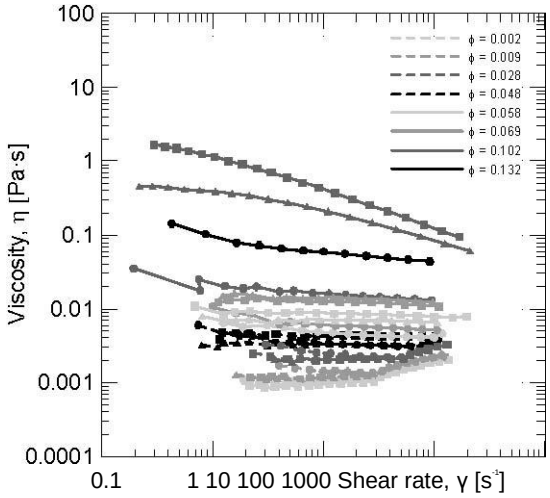

Figure 4. Rheograms of the nanofluids prepared. (⌘) *pH*=2, (☜) *pH*=7, (⇨) *pH*=10.

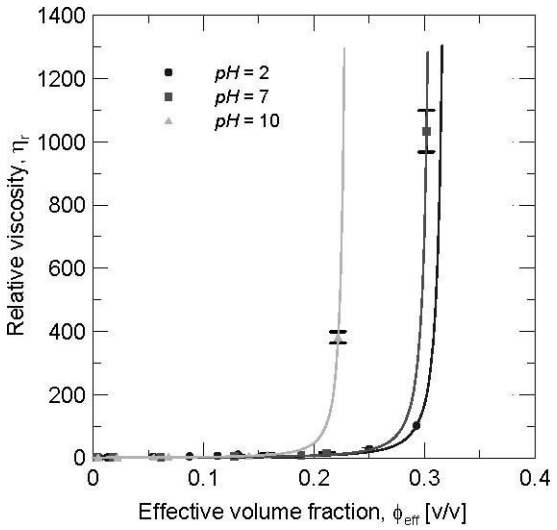

Figure 5. Evolution of relative viscosity with effective volume fraction and *pH*. Experimental data and modeled curve.

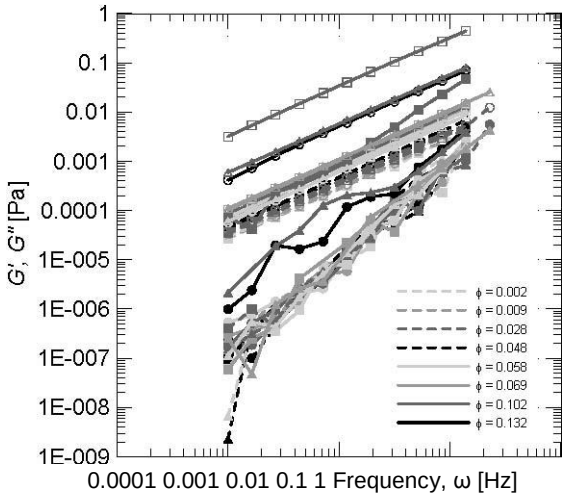

Figure 6. Evolution of elastic modulus (*G'*: solid symbol) and viscous modulus (*G''*: hollow symbol) with the oscillation frequency. (⌘) *pH*=2, (☜) *pH*=7, (⇨) *pH*=10.

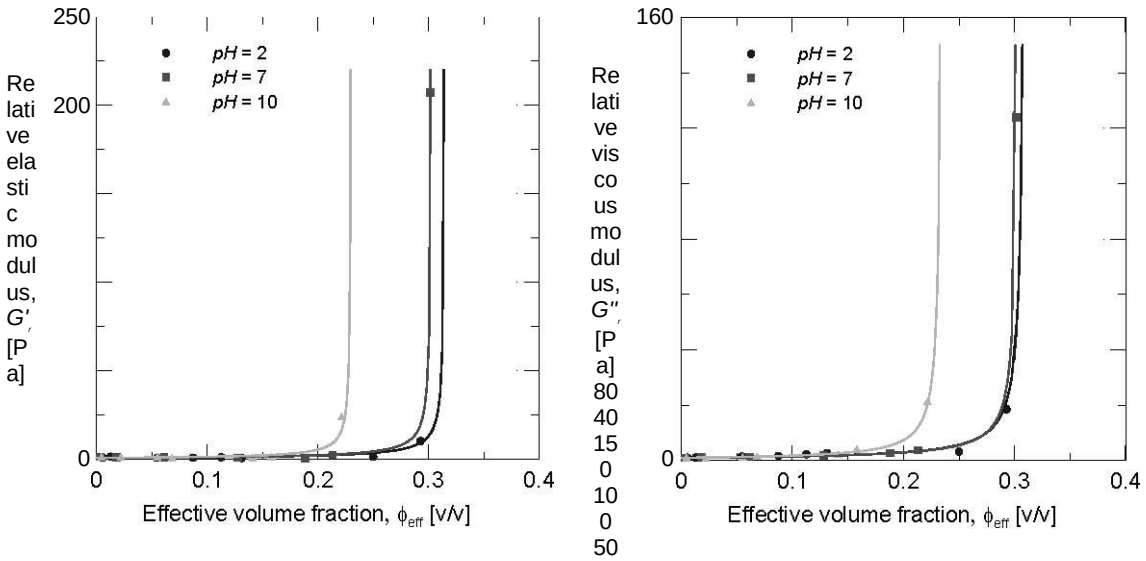

a) b)

Figure 7. Evolution of a) relative elastic modulus and b) relative viscous modulus with effective volume fraction and *pH*. Experimental data and modeled curve.

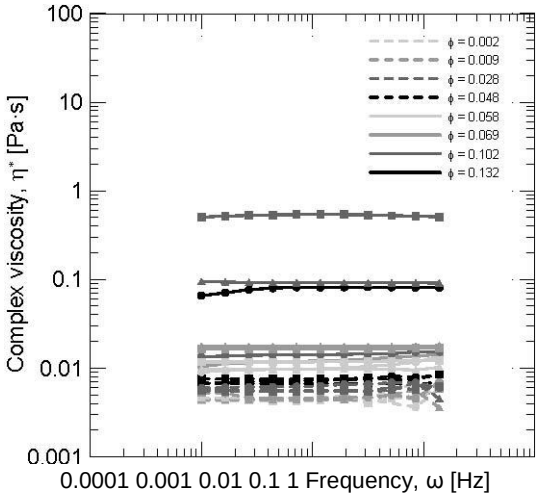

Figure 8. Evolution of complex viscosity with the oscillation frequency. (⌘) *pH*=2, (☜) *pH*=7, (⇨) *pH*=10.

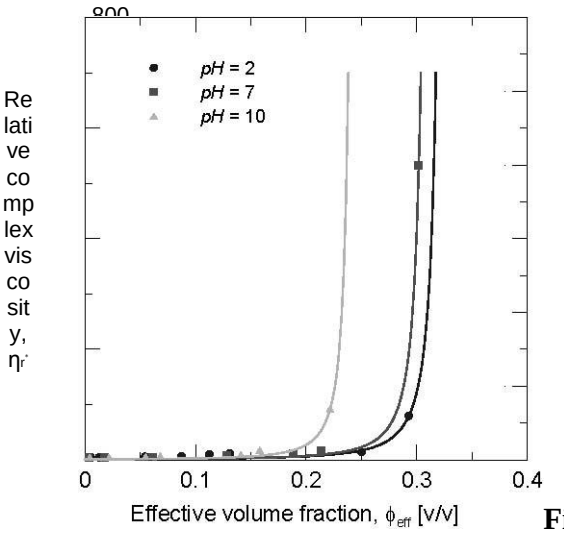

Figure 9. Evolution of relative complex viscosity with effective volume fraction and *pH*. Experimental data and modeled curve.

Table captions

Table 1. Evolution of yield stress and plastic viscosity with solid content and *pH*. Table 2. Electrical double layer and effective volume fraction. Table 3. Maximum packing fraction and intrinsic viscosity for each *pH* value. Viscosity model. Table 4. Maximum packing fraction for each *pH* value. Elastic modulus model. Table 5. Maximum packing fraction for each *pH* value. Viscous modulus model. Table 6. Maximum packing fraction and intrinsic viscosity for each *pH* value. Complex viscosity model.

Table 1. Evolution of yield stress and plastic viscosity with solid content and *pH*.

Table 2. Electrical double layer and effective volume fraction.

Cita bibliográfica / Cita bibliogràfica (ISO 690):

MONDRAGON, Rosa, et al. Determinatior packing fraction of silica nanoparticles fror rheological and viscoelastic measurements nanofluids. *Chemical Engineering Science*, vol. 80, p. 119-127.

Cita bibliográfica / Cita bibliogràfica (ISO 690):

MONDRAGÓN CAZORLA, Rosa, et al. Determin the packing fraction of silica naoparticles from rheological and viscoelastic measurements of nanofluids. *Chemical Engineering Science*, 201 p. 1.

MONDRAGÓN CAZORLA, Rosa, et al. Determin the packing fraction of silica naoparticles from rheological and viscoelastic measurements of nanofluids. *Chemical Engineering Science*, 201 p. 1.

ϕ_H $\sigma_Y \cdot 10_3$ **[Pa]** $\eta_P \cdot 10_3$ **[Pa·s]** R_2

Cita bibliográfica / Cita bibliogràfica (ISO 690):

MONDRAGOI
packing fractio
rheological and
nanofluids. *Che*
vol. 80, p. 119-

Cita bibliográfica / Cita bibliogràfica (ISO 690):

MONDRAGÓN C
the packing fract
rheological and v
nanofluids. *Chem*
p. 1.

MONDRAGÓN C
the packing fract
rheological and v
nanofluids. *Chem*
p. 1.

φ **[v/v]**	***pH***	$\sigma_Y \cdot 10^3$ **[Pa]**	$\eta_P \cdot 10^3$ **[Pa·s**

Table 3. Maximum packing fraction and intrinsic viscosity for each *pH* value. Viscosity model.

Cita bibliográfica / Cita bibliogràfica (ISO 690):

MONDRAGON, Rosa, et al. packing fraction of silica nan rheological and viscoelastic r nanofluids. *Chemical Engine* vol. 80, p. 119-127.

Table 4. Maximum packing fraction for each *pH* value. Elastic modulus model.

Table 5. Maximum packing fraction for each *pH* value. Viscous modulus model.

Cita bibliográfica / Cita bibliogràfica (ISO 690):

MONDRAGON, Rosa, et al. I
packing fraction of silica nanc
rheological and viscoelastic m
nanofluids. *Chemical Enginee*
vol. 80, p. 119-127.

Cita bibliográfica / Cita bibliogràfica (ISO 690):

MONDRAGON, Rosa, et al. I
packing fraction of silica nano
rheological and viscoelastic m
nanofluids. *Chemical Engineer*
vol. 80, p. 119-127.

Table 6. Maximum packing fraction and intrinsic viscosity for each *pH* value. Complex viscosity model.

Cita bibliográfica / Cita bibliogràfica (ISO 690):

MONDRAGON, Rosa, et al. packing fraction of silica nar rheological and viscoelastic nanofluids. *Chemical Engine* vol. 80, p. 119-127.